Numerical Simulation of Microdroplet Formation in Coflowing Immiscible Liquids

Jinsong Hua, Baili Zhang, and Jing Lou
Institute of High Performance Computing, 01-01 The Capricorn, Singapore Science Park II, Singapore 117528

DOI 10.1002/aic.11287
Published online August 31, 2007 in Wiley InterScience (www.interscience.wiley.com).

Monodisperse microdroplets can be formed when a liquid is injected via a capillary needle nozzle into another immiscible coflowing liquid in a microchannel. Such system has been applied in microfluidic devices to produce monodisperse microdroplets with controllable size. In this article, the drop formation in a coflowing system is simulated numerically using a front tracking/finite volume method to investigate the droplet formation mechanism. This numerical method solves a single set of Navier–Stokes equations for both liquid phases on a fixed Eulerian two-dimensional cylindrical coordinate mesh to account for the fluid flow dynamics. The front tracking method is applied to track the movement of the interface between the two immiscible liquids as well as the surface tension force. The simulation results demonstrate that the process of droplet formation in the coflowing immiscible liquids can be reasonably predicted. Two droplet generation modes (namely dripping and jetting), which have been observed in experiments, are successfully produced through the numerical simulations under certain flow conditions. Moreover, the effects of the continuous phase flow speed, viscosity, and the interface tension on the droplet size are investigated. The correlation of the nondimensional droplet size (r_d^*) with the continuous phase flow parameters such as the Reynolds number (Re_o), Weber number (We_o), Capillary number (Ca_o), and viscosity ratios (μ^*) can be obtained as $r_d^* \propto Ca_o^{-1/2} Re_o^{-1/6}$ for the dripping mode and as $r_d^* \propto Ca_o^{1/3} We_o^{-1/2} \mu^{*-1/2}$ for the jetting mode from the current simulations. *AIChE J,* 53: 2534–2548, 2007
Keywords: multiphase flow, numerical simulation, front-tracking method, monodisperse droplet, droplet formation, coflowing fluid

Introduction

Droplets of one fluid dispersed in a second immiscible fluid are useful in a wide range of applications, particularly when the droplet size can be prescribed at micro- or nanoscale and the droplet size distribution is narrow. For example, liquid emulsions are widely applied in the industries of food, cosmetics, pharmaceutics, and polymers. Recently, demand of nearly monodisperse emulsions has been rising due to the recent advances in the production of microcapsules or specially structured multiphase systems. The formation of microdroplet also has very important roles in applications of BioMEMS and Lab-on-Chip. Some emerging technologies and processes as reviewed in the works by Basaran[1] and Barrero and Loscertales[2] are developed to make monodisperse droplets with controllable size.

Anna et al.[3] presented a range of droplet formation behavior from experiments in a microfluidic flow-focusing device with rectangular cross-section channels, in which the inner and outer flow streams are water and oil, respectively. They studied on the effects of the liquid phase flow rates on the droplet formation pattern. Xu and Nakajima[4] presented another configuration of a "flow-focusing" microchannel to generate highly monodisperse droplets with diameter much

Correspondence concerning this article should be addressed to Dr. J. Hua at huajs@ihpc.a-star.edu.sg.

smaller than the width of the channel junction, without applying additional perturbations. Through control of the flow rate ratios, the eventual break-up of the dispersed liquid phase occurs as the flow is focused to a critical break up width. Xu et al.[5] described a versatile strategy for producing monodisperse solid particles with sizes from 20–1000 μm. Their method involves the formation of monodisperse liquid droplets by using a microfluidic device, shaping the droplets in a microchannel, and then solidifying these droplets in situ either by polymerizing a liquid monomer or by lowering the temperature of a liquid that sets thermally. Utada et al.[6] proposed a method to produce double emulsions using multiple streams of coaxial flows through microcapillary nozzles in a microchannel. In all these state-of-the-art fabrication technologies, the generation of highly monodisperse droplets is one of the core technical issues in these microfluidic devices to produce particles with uniform microstructures. Hence, the fundamental understanding of the hydrodynamic mechanism governing the breakup of a liquid stream into monodisperse droplets under a confined microchannel with a coflowing liquid are essential to the success of applying these fabrication technologies to industrial applications.

Although the breakup of capillary streams in open macroscopic environments has been studied by Zhang and Stone,[7] Zhang and Basaran,[8] and Zhang,[9,10] the breakup of a liquid stream in a confined microchannel with coflowing liquid environment is still poorly understood. Cramer et al.[11] studied experimentally the droplet formation at a capillary tip in a coflowing ambient fluid. The droplet formation is affected by the flow rates of the continuous and the dispersed phases, fluid viscosity, and interfacial tension. Umbanhowar et al.[12] introduced a technology to produce highly monodisperse emulsions by introducing the dispersed phase into a coflowing stream via a tapered capillary. Drops detach from the capillary when the streamwise forces exceed the force due to interfacial tension. Garstecki et al.[13] presented a qualitative analysis on the liquid stream breakup in a viscous coflowing liquid through a confined geometry of a long and narrow orifice. Since the drop formation mechanism in a coflowing system is affected by a number of parameters, such as flow speed, viscosity, and capillary force as well as the confinement of microchannel wall, it is difficult to obtain a deep understanding of such complex problem if just relying on experimental investigation and theoretical analysis. The first principle based numerical simulation provides a wonderful alternative solution to such complex problem. The development of a numerical model will not only help us understand the dominant factors on the drop formation mechanism, but also provide a tool for the microdevice system design.

In the previous works of Zhang,[9,10] numerical simulations have been used to investigate the drop formation dynamics of a viscous liquid at the tip of a vertical, circular tube into an viscous ambient fluid due to the gravitational force. A volume-of-fluid/continuum-surface-force (VOF–CSF) method was developed to predict the evolution of drop shape and its breakup mechanism. It solved the Navier–Stokes equations using finite-difference formulation on a fixed Eulerian mesh. The interface was tracked using a function of the volume fraction of fluid, which captured the moving interface and the topology change resulted by interface breakup and coalescence. Wilkes et al.[14] also performed a numerical study on the dynamics of formation of a Newtonian liquid drop from a capillary tube into an ambient gas phase. In their modelling, the transient Navier–Stokes equations subject to appropriate initial and boundary conditions were solved using a finite element method in a two dimensional axisymmetric domain to analyze the drop growth dynamics at finite Reynolds numbers. The algorithm could capture not only the gross features of the phenomena involved, such as the limiting liquid thread length at the breakup of a drop and the volume of the primary drop, but also its fine features, such as a microthread that develops from a main thread or a neck in a viscous drop approaching breakup. Further quantitative comparisons among simulations, experiments, and scaling theories by the same research group were reported in the work by Chen et al.[15] Numerical simulation of droplet formation using flow focusing in microchannels can be found in the work of Davidson et al.[16] They used VOF method to predict the dynamics of drop formation in an axisymmetric microfluidic flow-focusing geometry for an immiscible liquid–liquid system. They concluded that both ending pinching and capillary-wave instability were important for droplet breakup from the liquid jet with high flow rate. Recently, Suryo and Basaran[17] studied the liquid droplet formation from a tube in a coflowing outer fluid through numerical simulation. It was found that the droplet size can be reduced, even leading to tip streaming, when increasing the ratio of the outer liquid flow rate to the inner liquid flow. Zhou et al.[18] studied numerically the breakup of simple and compound jets in a flow-focusing channel. A finite element method was used to solve the Navier–Stokes equation on an unstructured triangular, adaptive mesh. They successfully reproduced the scenarios of jet breakup and drop formation previously observed in experimental flow-focusing devices. They also elucidated the effects of flow rate and rheological parameters on the drop formation process and final drop size.

A state-of-the-art front tracking method, which is a hybrid approach of the front capturing and front tracking technique proposed by Unverdi and Tryggvason,[19] has been examined, further extended and validated by Hua et al.[20,21] In this article, this method is applied to investigate the microdroplet formation in a coflowing liquid. A stationary, fixed grid is used for the fluid flow, and a set of adaptive elements on the front is used to mark the interface. A single set of governing equations (Navier–Stokes equation) is solved for the whole computational domain, treating the different phases as one fluid with variable material properties. The fluid properties such as density and viscosity are calculated based on the position of the interface. Interfacial source terms such as interface tension are computed on the interface between the two phases and distributed to the fixed grid using a dirac-delta function. The transient incompressible Navier–Stokes equations are discretized by a finite volume scheme on the fixed, staggered, structured grid, and solved numerically using SIMPLE algorithm.[22] The interface is tracked explicitly using the advection velocity interpolated from the fixed background grid. The fluid properties are then updated according to the movement of the immiscible fluid interface.

The objectives of this study are two folds. One is to evaluate the capability of the front tracking method to simulate the microdroplet formation in the coflowing viscous immiscible fluids. The other is to investigate the effects of

some flow parameters, such as liquid flow rate and fluid property, on the drop formation dynamics. The rest of the article is organized as follows. The mathematical formulation of the governing equations, boundary conditions, treatment of the fluid interface, and the numerical method are presented in the following section. Then, a validation study is presented to simulate liquid droplet formation in an immiscible quiescent liquid environment using the current front tracking method.[21] Subsequently, the numerical model is used to simulate the typical drop formation processes in both dripping and jetting modes, showing the droplet shape evolution and breakup and flow field variation. The effects of the flow rate and fluid parameters (e.g., viscosity and interfacial tension) on the drop formation are investigated numerically and discussed. Finally, the conclusions drawn from this study are summarized.

Mathematic Formulation and Numerical Method

Problem description

A typical coflowing system of two viscous immiscible liquids is illustrated in Figure 1. The dispersed liquid (Fluid 1) is injected through a capillary nozzle with a radius of R_i into a coflowing liquid (Fluid 2) in a coaxial cylindrical tube with an inner radius of R_o. The gravitational force aligns with the axis of the tube and nozzle. The disperse phase (drop liquid) is injected into the system continuously at a constant flow rate of Q_i, and the continuous phase (coflowing liquid) at a constant flow rate of Q_o. The fully developed laminar velocity profile is applied to the inlets for the inner liquid and the outer liquid through the boundary conditions. The length of the computational domain is about 30 R_i, which is sufficiently long for all the results to be reported in this article. The outlet of the inner capillary nozzle is located about one R_i downstream from the outer tube inlet. The fluid properties such as density and viscosity for both phases are assumed to be constant while they flow through the system. As the two fluid phases are immiscible, an axis-symmetric interface is formed between two streams. The interface evolves, collapses, and forms droplets when the two immiscible liquid phases are flowing through the system. Because of the low Reynolds number for the flow in microfluidic devices, the system can be reasonably represented by a two dimensional axisymmetric model.

Governing equations and boundary conditions

For a multifluid system, the mass and stress balances on the interface between two fluids may be described as follows[23] if the two fluids can be considered as incompressible. Firstly, the normal velocity in each fluid phase on the interface should be continuous, and can be expressed as

$$[\mathbf{u}] \cdot \mathbf{n} = 0, \tag{1}$$

in which the square brackets represent the jump across the interface, $\mathbf{u}$ is the fluid velocity, and $\mathbf{n}$ represents the unit normal vector to the interface. Secondly, a stress balance on the interface may be expressed as

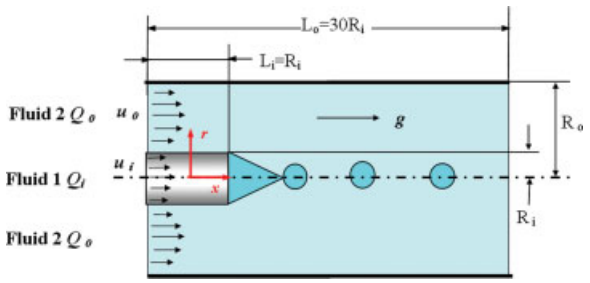

Figure 1. Schematic of droplet formation from the tip of a capillary tube in a coflowing viscous liquid (not to scale).

[Color figure can be viewed in the online issue, which is available at www.interscience.wiley.com.]

$$[-p + \mu(\nabla\mathbf{u} + \nabla\mathbf{u}^T)] \cdot \mathbf{n} = \sigma\kappa\mathbf{n}, \tag{2}$$

$$[\mu(\nabla\mathbf{u} + \nabla\mathbf{u}^T)] \cdot \mathbf{t} = 0, \tag{3}$$

where p is the pressure in the fluid domain, σ is the surface tension, κ is the curvature of the interface, t the unit tangent vector at the interface, and μ the fluid viscosity.

In this study, it is reasonable to treat the liquid phase as incompressible fluid. Hence, the mass conservation equation on the whole domain (both fluid phases and the interface) can be expressed by

$$\nabla \cdot \mathbf{u} = 0. \tag{4}$$

The Navie–Stokes equation, governing the momentum balance in each fluid phase and on the interface, can be expressed as,

$$\frac{\partial(\rho\mathbf{u})}{\partial t} + \nabla \cdot \rho\mathbf{u}\mathbf{u} = -\nabla p + \nabla \cdot [\mu(\nabla\mathbf{u} + \nabla\mathbf{u}^T)] + \int \sigma\kappa\,\mathbf{n}\,\delta(\mathbf{x} - \mathbf{x}_f)ds + (\rho - \rho_o)\mathbf{g}, \tag{5}$$

where, $\delta(\mathbf{x} - \mathbf{x}_f)$ is a delta function that is zero everywhere except at the interface, $\mathbf{g}$ is the gravitational acceleration, and subscript f refers the interface. ρ is the fluid density, and ρ_o the density of the continuous liquid phase.

The transient Navier–Stokes equations are solved for the drop formation, beginning at the instant at which the free surface of drop is flat and situates at the tip of the inner capillary tube and the entire system is assumed to be initially rest. The following boundary conditions are applied to solve the governing equations. In this study, we assume that the wall thickness of capillary tube is sufficiently thin comparing to the tube inner diameter. The interface between the two immiscible liquid phases is always pinned on the sharp end of the capillary tube.

At the upstream of the inner capillary tube, a fully developed laminar flow velocity profile is set as

$$\begin{cases} V_i = 0 \\ U_i(r) = \dfrac{2 \cdot Q_i}{\pi R_i^2}\left[1 - \left(\dfrac{r}{R_i}\right)^2\right] \end{cases} \quad \text{for} \quad 0 \le r \le R_i, \tag{6}$$

where, V_i and U_i are the radial and axial component of the velocity of the dispersed (inner) liquid, respectively.

Similarly, a fully developed laminar flow is imposed on the upstream annulus of the outer continuous liquid phase

$$\begin{cases} V_o = 0 \\ U_o(r) = \dfrac{2 \cdot Q_o}{\pi(R_o^2 - R_i^2)} \times \dfrac{1 - \left(\dfrac{r}{R_o}\right)^2 + \dfrac{1 - (R_i/R_o)^2}{\ln(R_o/R_i)} \ln(r/R_o)}{\left(1 + \dfrac{R_i}{R_o} - \dfrac{1 - (R_i/R_o)^2}{\ln(R_o/R_i)}\right)} \end{cases}$$

$$\text{for } R_i \le r \le R_o, \quad (7)$$

where, V_o and U_o are the radial and axial component of the velocity of the continuous (outer) liquid phase, respectively. The averaged flow speed in the inner tube can be expressed as $u_i = Q_i/\pi {R_i}^2$ and in the outer annular channel as $u_o = Q_o/\pi(R_o^2 - R_i^2)$.

On all the solid walls, no-slip and no penetration boundary conditions are applied. A symmetry boundary condition is applied along the central axis. Hence, only half of the domain shown in Figure 1 is solved in the numerical simulations. An outflow boundary condition is applied at the right most boundary of the solution domain. The axial length of the simulation domain is about 30 times of the inner capillary nozzle radius, which is sufficiently longer than the estimated drop pinch-off distance.

On the basis of the above description of the problem and the governing Eq. 5, it can be concluded the flow field can be expressed as a function of the following 10 variables: u_o, u_i, R_o, R_i, ρ_o, ρ_i, μ_o, μ_i, σ, and g. To simplify the problem parameter setting, we introduce the following dimensionless variables,

$$x^* = \frac{x}{R_i}; \quad r^* = \frac{r}{R_i}; \quad u^* = \frac{u}{u_i}; \quad \tau = \frac{t}{R_i/u_i}; \quad \rho^* = \frac{\rho}{\rho_i};$$
$$p^* = \frac{p}{\rho_i {u_i}^2}; \qquad \mu^* = \frac{\mu}{\mu_i}; \qquad \kappa^* = \frac{\kappa}{R_i^{-1}}; \qquad \mathbf{g}^* = \frac{\mathbf{g}}{{u_i}^2/R_i}$$

where, the radius of the capillary nozzle for the disperse phase, R_i, is used as the characteristic length, and the average flow speed of the inner disperse liquid phase (u_i) is used as the characteristic velocity. And they are used to normalize the Navier–Stokes Eq. 5. Hence, the nondimensional Navier–Stokes equation may be re-expressed as

$$\frac{\partial(\rho \mathbf{u}^*)}{\partial t} + \nabla \cdot \rho \mathbf{u}^* \mathbf{u}^* = -\nabla p^* + \frac{1}{Re^*} \nabla \cdot [\mu^* (\nabla \mathbf{u}^* + \nabla {\mathbf{u}^*}^T)] + \frac{1}{We^*} \int \kappa_f^* \mathbf{n}_f \delta(\mathbf{x}^* - \mathbf{x}_f^*) ds + (\rho^* - 1)\mathbf{g}^* \quad (8)$$

The nondimensional parameters such as Reynolds number and Weber number are defined as follows

$$Re^* = \frac{\rho_i u_i R_i}{\mu_i}; \quad We^* = \frac{\rho_i u_i^2 R_i}{\sigma}. \quad (9)$$

On the basis of the above formulation, the problem of microdroplet formation in a coflowing liquid could be characterized by the following nondimensional parameters, namely, the ratios of density ($\rho^* = \rho_o/\rho_i$) and viscosity ($\mu^* = \mu_o/\mu_i$) of two fluids, Reynolds number (Re^*), Weber number (We^*), the flow velocities or flow rates of two liquid phases ($\overline{u}_i{}^* = 1.0$, $\overline{u}_o{}^* = u_o/u_i$), and the geometrical size ratio of the outer tube to the inner capillary nozzle (R_o/R_i). Even though the gravitational force normally does not have significant effects in micro fluidic flows, the gravitational force term is not neglected in the governing Eq. 8 in the current study. This is because of the fact that a case study[9] of buoyancy induced droplet pinch off behavior is used as the validation case in this article. Therefore, the following set of dimensionless numbers: $\overline{u}_0^*$, R_o/R_i, ρ^*, μ^*, g^*, Re^*, and We^* will be used as the input parameters for the simulations.

A number of dimensionless parameters for the continuous phase have been defined to indicate the importance of viscous force, inertial force, and gravitational force in the multiphase flows. The Weber number (We_o) is defined as the ratio of inertia to surface tension $We_o = \frac{\rho_o u_o^2 R_i}{\sigma}$. The Capillary number ($Ca_o$) is defined as the ratio of viscous force to surface tension ($Ca_o = \frac{u_o \mu_o}{\sigma}$). The ratio of the inertia to viscous force is expressed as Reynolds number $Re_o = \frac{We_o}{Ca_o} = \frac{\rho_o u_o R_i}{\mu_o}$. Taking into account the nondimensionalization applied to the basic governing equations, these dimensionless parameters can be expressed using the simulation input parameters ($\overline{u}_o^*$, R_o/R_i, ρ^*, μ^*, g^*, Re^*, and We^*)

$$We_o = \frac{\rho_o u_o^2 R_i}{\sigma} = \frac{\rho_o \overline{u}_o^{*2} u_i^2 R_i We^*}{\rho_i u_i^2 R_i} = \rho^* \overline{u}_o^{*2} We^*, \quad (10)$$

$$Ca_o = \frac{u_o \mu_o}{\sigma} = \frac{\overline{u}_o^* u_i \mu^* \mu_i We^*}{\rho_i u_i^2 R_i} = \frac{\overline{u}_o^* \mu^* We^*}{Re^*}, \quad (11)$$

$$Re_o = \frac{\rho_o u_o R_i}{\mu_o} = \frac{\rho^* \rho_i \overline{u}_o^* u_i R_i}{\mu^* \mu_i} = \frac{\rho^* \overline{u}_o^* Re^*}{\mu^*}. \quad (12)$$

One of the objectives in this study is to investigate the dependence correlation of droplet size with these dimensionless flow parameters. The nondimensional droplet size is defined as $r_d^* = R_d/R_i$.

Interface treatment and tracking

The distributions of fluid properties (density and viscosity) over the whole solution domain are required to solve the Navier–Stokes equations over a fixed grid. Although the density and viscosity of each fluid is constant, the abrupt jump across an interface may lead to either excessive numerical diffusion or numerical instability. The novelty of the front tacking method proposed by Tryggvason's group[19] is that the front is considered to have a finite thickness of the order of the fixed background mesh size instead of zero thickness. In the transition zone around the interface, the fluid properties change smoothly and continuously from the value on one side of the interface to the value on the other side. The artificial thickness of the front depends on the grid size, and is kept constant during the computation. Hence, this method does not have numerical diffusion across the interface. The material property fields over the whole domain may be reconstructed using an indicator function $I(\mathbf{x},t)$, which has the value of one in the one liquid phase and zero in another liquid phase at a given time t.

$$b(\mathbf{x},t) = b_i + (b_o - b_i)I(\mathbf{x},t)\,; \tag{13}$$

$$I(\mathbf{x},t) = \int_{\Omega(t)} \delta(\mathbf{x}-\mathbf{x}')da, \tag{14}$$

in which b stands for either fluid density or viscosity, and the subscripts i and o stand for the inner and outer liquids, respectively. The indicator function can be written in the form of an integral of the $\delta(\mathbf{x}-\mathbf{x}')$ function over the domain ($\Omega(t)$) bounded by interface $\Gamma(t)$. $\delta(\mathbf{x}-\mathbf{x}')$ is a delta function that has a value of zero anywhere else except on the interface. In this study, the delta function is approximated by the following distribution function $D(\mathbf{x})$ suggested by Peskin and Printz[24] for a two-dimensional grid system

$$D(\mathbf{x}-\mathbf{x}_f) = \begin{cases} (4h)^{-2}\prod_{i=1}^{2}\left(1+\cos\left(\frac{\pi}{2h}|\mathbf{x}_i-\mathbf{x}_{i,f}|\right)\right), & \text{if } |\mathbf{x}_i-\mathbf{x}_{i,f}| < 2h \\ 0, & \text{otherwise.} \end{cases} \tag{15}$$

where h is the grid size of the background mesh and i stands for the two directions of the coordinate system. The distribution function defines the fraction of the interface quantity that can be assigned to nearby grid points across the artificial thickness of the front.

When the fluid velocity is updated on the fixed grid, the node moving velocity on the front could be computed by interpolating from the fixed background grid to ensure that the front moves at the same velocity as the surrounding fluids. The distribution function has been used to spread the fluid property jump to the fixed points near the interface. Similarly, this function can also be used to interpolate field variables from the stationary fixed background grid to the front using the following equation

$$\mathbf{u}_f = \sum D(\mathbf{x}_f - \mathbf{x})\mathbf{u}(\mathbf{x}). \tag{16}$$

Then, the front is advected along its normal direction in a Lagrangian fashion

$$\mathbf{x}_f{}^{n+1} - \mathbf{x}_f{}^{n} = \Delta t\,\mathbf{u}_f. \tag{17}$$

After the position of the front is updated, the sizes of the front elements that are associated with front marker nodes may have been modified as well. Hence, the front elements are adapted to maintain the element quality. In the present work, an axisymmetric model is applied, and the interfacial front is marked by a set of connected line elements. In this study, the front consists of 4–10 line elements within one fixed background grid cell.

Numerical method

A projection method for the integration of the Navier–Stokes Eq. 8 was used in the previous works of Unverdi and Tryggvason.[19] The difficulties in solving the pressure equation have been reported in the literature.[25] For example, a large density ratio may lead to the difficulty in convergence. To overcome the difficulties in solving the pressure equation, an alternative approach[20,21] is implemented. Here, the coupling fluid velocity and pressure is updated by solving the momentum equations and continuity equation using SIMPLE scheme.[22] In the multifluid system, since there is density jump over the phase interface, mass flux conservation in the control volume crossing the front interface is not valid. Hence, volume flux conservation is adopted to modify the SIMPLE algorithm.[21] On the basis of this approach, the SIMPLE algorithm is used to calculate the correction value of pressure and velocity after solving the momentum equation.

Solution procedure

With appropriate initial conditions for the fluid flow and interface shape, the solution algorithm proceeds iteratively through the following steps:

1. Using the fluid velocity field ($\mathbf{u}^n$) and the interface position ($\mathbf{x}_f^n$), the moving velocity of the front marker points ($\mathbf{u}_f^n$) is computed using Eq. 16.
2. Using the estimated interface velocity ($\mathbf{u}_f^n$), the front is advected to the new position ($\mathbf{x}_f^{n+1}$). Subsequently, the elements, representing the front, are examined for adaptation and topology change.
3. At the new interface positions, the redistribution of the interface property is performed with the reconstructed indicator function $I(\mathbf{x}_f^{n+1})$. Hence, new fluid property field such as density (ρ^{n+1}), viscosity (μ^{n+1}), as well as the surface tension are obtained.
4. With appropriate wall boundary conditions, the momentum equation and mass continuity equation can be solved using the modified SIMPLE algorithm. This leads to update fluid velocity ($\mathbf{u}^{n+1}$) and pressure (p^{n+1}).
5. Repeat the solution steps from (1) to (4) for the next time step calculation.

A uniform background grid of 600 × 60 has been used in the current simulation using an axisymmetric model. The outlet of the inner nozzle is resolved with 20 grid points. According to the grid sensitivity analysis presented in the previous work,[21] the background grid resolution is fine enough to produce grid-independent results. In addition, a constant, nondimensionalized time step size around 0.002 is used in the simulation, which is small enough to capture the temporal variation of the droplet formation dynamics of the primary droplets. The simulation duration is also long enough to capture the droplet formation dynamics when the droplet generation process can be stably repeated. In the present study, each simulation produces at least 10 primary droplets. The simulation is performed on an IBM p575 super computer. The simulation time normally takes about 10–20 CPU-hours.

Validation of numerical simulation method

Both experimental and numerical studies on the liquid droplet formation in an immiscible quiescent liquid environment were reported in the past work of Zhang.[9] The experiments have been designed to obtain quantitative information on the dynamics of drop formation of a typical liquid–liquid system of 2-ethyl-1-hexanol drops forming and breaking into distilled water. The apparatus used to form drops has been described elsewhere.[8] The liquid drop is formed at or emerged from the tip of a capillary tube, which are submerged in water container having sufficient large inner diameter as compared with the capillary tube radius. The VOF/

CSF based numerical simulations have also been performed by Zhang[9] to simulate the complete process of drop formation from the time a drop emerges from the tube to its break off from the tube with continuous feeding of the drop liquid at a certain flow rate. In this article, the front tracking method[21] is applied to simulate the same drop formation process. The inner radius of the capillary tube is about 0.16 cm. The drop liquid, 2-ethyl-1-hexanol, has the viscosity and density of 0.089 Pa·s and 830 kg/m^3, respectively. The ambient liquid, distilled water, has a viscosity and density of 0.001 Pa·s and 997 kg/m^3, respectively. The interfacial tension is measured to be 0.0132 N/m. Figure 2 shows the comparison of drop evolution observed in the experiments[9] and predicted using the current numerical simulation method. The current numerical method can make reasonable prediction on the liquid drop forming process in another quiescent immiscible liquid due to the buoyancy as a result of the density difference between two liquid phases. In addition, extensive validations of the current numerical method for modeling two-phase flow, e.g., bubble rising in quiescent liquid, against experiments in a wide flow regime have also been reported by Hua and Lou.[21]

In the process of droplet formation, the break-up of the necking liquid thread also plays an important role. In view of drop pinch-off/snap-off physics, the breaking up dynamics may depend upon the flow conditions at the place where liquid thread necking occurs (e.g., distributions of flow speed and pressure, fluid flow inertia), liquid property (e.g., density and viscosity), and interface property (e.g., surface tension). The dynamics of the drop formation and pinch-off has been investigated extensively in the faucet dripping,[14,15,26,27] but is still a challenge in mathematical modeling.[28] Hence, in the current simulation, a simple interface rupture model is adopted to break the liquid interface when it comes within a very small distance (Δd) from the symmetric axis. A similar modeling strategy has also been adopted in the works of Homma et al.[29] and Jensen et al.[30] The drop breaking distance (Δd) is chosen on an ad hoc basis as half of the grid size of the background mesh used for the flow field solution in the present study. As shown in Figures 2f, g, it is found that the formation of the primary drop has less dependence upon the breaking distance. However, the formation of satellite drop does strongly depend upon the breaking distance chosen. The emphasis in this study is focused on how the dynamics of the primary drops formed in the coflowing liquids and how the size of the primary drop is affected by the liquid properties and flow conditions.

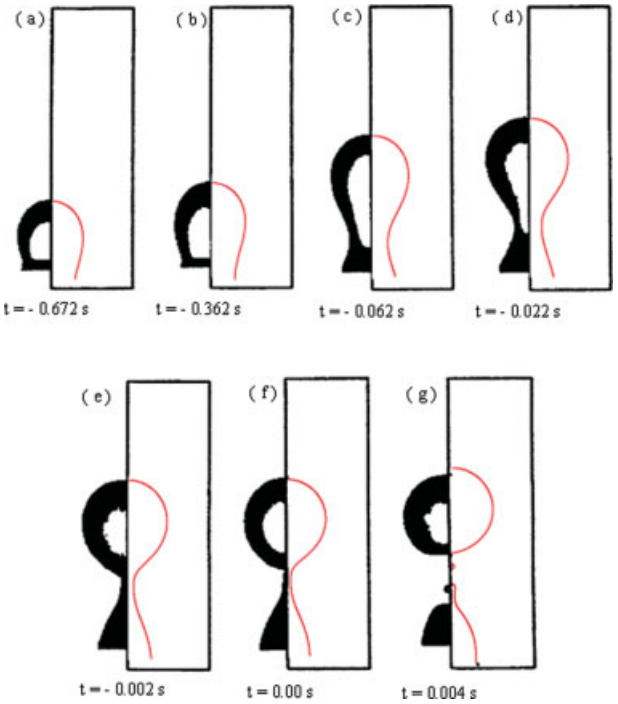

Figure 2. Comparison of the drop evolution observed in experiment[9] and prediction by the present simulation.

[Color figure can be viewed in the online issue, which is available at www.interscience.wiley.com.]

Table 1. Typical Ranges of the Parameters Used in Experiments[6,11] for Microfluidic System and the Dimensionless Numbers Applied in the Simulation

	Parameter	Typical Value
Experimental parameters	Diameter of the capillary nozzle	100–200 μm
	Diameter of the outer microchannel	300–600 μm
	Flow speed of the continuous liquid phase	0.02 –1.0 m/s
	Flow speed of the dispersed liquid phase	0.01–0.05 m/s
	Surface tension	20–70 mN/m
	Liquid viscosity	0.001–0.3 Pa s
	Liquid density	800–1000 kg/m^3
Dimensionless numbers	Diameter ration of the outer channel to the capillary nozzle	$R_o/R_i = 3.0$
	Density ratio	$\rho^* = 0.8$
	Flow speed of the disperse liquid phase	$\bar{u}_i^* = 1.0$
	Flow speed of the continuous liquid phase	$2.0 < \bar{u}_o^* < 20.0$
	Viscosity ratio	$0.5 < \mu^* < 5.0$
	Weber number (We_o)	$0.0030 < We_o < 0.078$
	Capillary number (Ca_o)	$0.035 < Ca_o < 0.35$
	Reynolds number (Re_o)	$0.01 < Re_o < 10.0$
	Bond number (Bo^*)	$0.0001 < Bo^* < 0.002$

Results and Discussion

The typical ranges of the operation parameters used in the experimental works on drop formation in a coflowing ambient fluid[11,12] and in flow-focusing devices[3,6] are listed in Table 1. Accordingly, the ranges of the dimensionless operation parameters such as Reynolds number, Weber number, viscosity ratio, and flow speed ratio introduced in the previous section to characterizing the multiphase flow system are also listed in Table 1. The simulations presented in this study will focus on the effects of the continuous liquid phase flow conditions, e.g., the average flow speed ($\bar{u}_o^*$), viscosity ratio (μ^*), and surface tension (Weber number We^*), on the size of

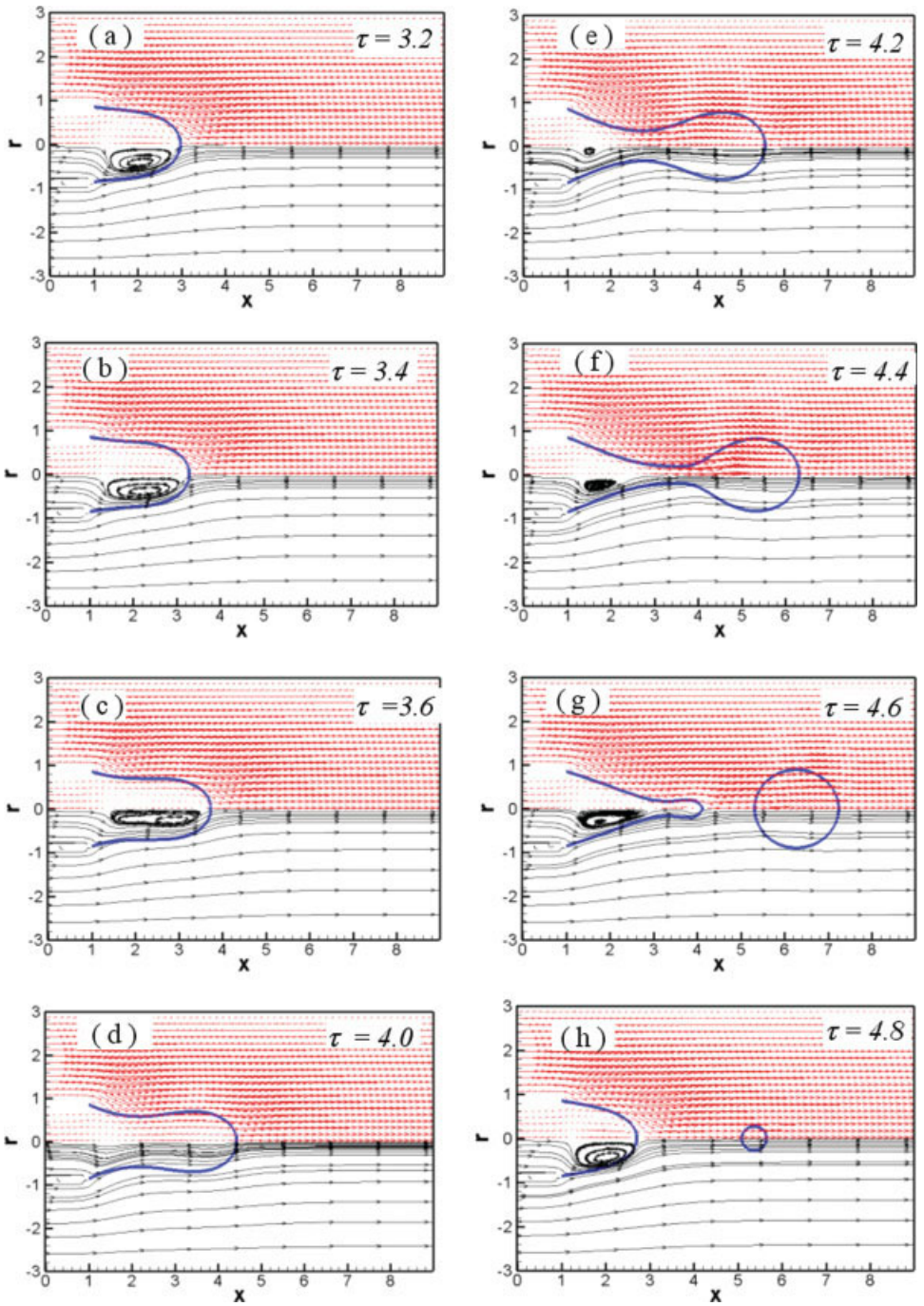

Figure 3. Simulation predicted temporal variation flow field and streamlines while droplet formation using coflowing immiscible liquids in the dripping mode.

The flow parameters are as follows: $\bar{u}_i = 1.0$, $\bar{u}_o^* = 5.59$, $Re^* = 0.0698$, $We^* = 0.00253$, $\rho^* = 0.9$, $\mu^* = 1.8$ and $R_o/R_i = 3.0$. [Color figure can be viewed in the online issue, which is available at www.interscience.wiley.com.]

primary droplet formed in a coflowing system. The flow conditions of the disperse liquid phase of the coflowing system are kept fixed ($\bar{u}_i^* = 1.0$, $Re^* = 0.1$, $g^* = 1.0$, and $\rho^* = 0.8$) for the most simulations presented in this article, as well as the radius ratio of the inner capillary nozzle to the outer channel ($R_o/R_i = 3.0$), unless they are specified with other values. As shown in Table 1, both Reynolds number and Weber number (smaller than 1.0) are relatively small for the microfluidic system. Hence, it can be concluded from the Eq. 8 that the gravitational force will not play a key factor on droplet formation in the microfluidic system. Since the inclusion of the gravitational force is quite easy and natural in the current numerical method, and it is important for the validate case presented in the previous section, the gravitation force term is included in the governing Eq. 8, but its effects on drop formation in microchannel flows is negligible.

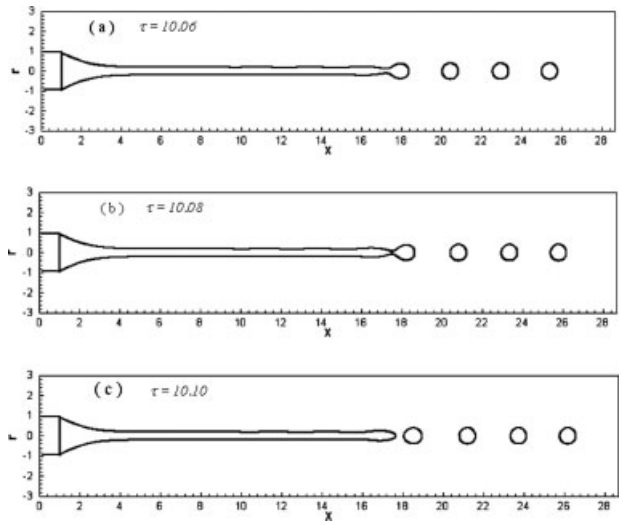

Figure 4. Simulation predicted droplet formation process from the tip of liquid jet of coflowing immiscible liquids in the jetting mode.

The flow parameters are as follows: $\bar{u}_i = 1.0$, $\bar{u}_o = 9.5$, $Re^* = 0.1$, $We^* = 0.001$, $\rho^* = 0.8$, $\mu^* = 1.5$ and $R_o/R_i = 3.0$.

Dynamics of droplet formation in microchannel

Experiments[6,11] have revealed that there are two modes of the droplet formation, namely dripping mode and jetting mode, in the coflowing system. In the dripping mode, the droplets are formed in the downstream nearby the capillary nozzle. In the jetting mode, the droplets are formed in the far downstream from the capillary nozzle. These two droplet formation modes associated with different droplet formation mechanisms[26] are explored in the current simulations under different flow conditions.

Figure 3 illustrates the simulation predicted temporal variation flow field and streamlines while droplet formation using coflowing immiscible liquids in the dripping mode under the flow conditions of $\bar{u}_i^* = 1.0$, $\bar{u}_o{}^* = 5.59$, $Re^* = 0.0698$, $We^* = 0.00253$, $\rho^* = 0.9$, $\mu^* = 1.8$ and $R_o/R_i = 3.0$. In Figure 3, the upper part shows the flow vector of flow field in both liquid phases, and the lower part shows the flow pathlines in both liquid phases. The simulation reveals the key phenomena during the droplet formation process in a microchannel such as the drop growth, necking, breakup of primary drop, and then satellite drop. As the continuous liquid phase flows into the microchannel from the outer annulus at a higher velocity, it produces viscous force on the interface between the two fluids. A circulating flow is induced inside the liquid tip of the dispersed fluid phase as shown in Figure 3a. As more dispersed liquid phase is injected into the microchannel, the front tip of the dispersed liquid phase moves downstream, which induces a larger interface area between the continuous phase and the disperse phase liquid. As a result, more momentum is transferred from the continuous liquid phase to the dispersed phase through viscous drag, which strengthens the flow along the continuous phase flow direction and weakens the circulation flow within the disperse liquid phase as shown in Figures 3b, c. The dispersed phase inside the interface front finally flows along the continuous liquid phase and is accelerated by the viscous drag force. As the interface front is dragged further forward and the dispersed phase velocity is increased further, the necking of the liquid thread is started to conserve flow rate of disperse phase within the interface as shown in Figure 3d. On the one hand, the necking of liquid thread may lead to higher drag force on the front part of the liquid thread. On the other hand, the necking may cause higher capillary pressure inside the necking region of liquid thread due to the higher curvature at the necked interface. The high capillary pressure pushes the front part of the dispersed liquid phase flow forward, slows down the rear part of the dispersed liquid as shown in Figure 3e. Finally, breaking off the liquid thread at the position of neck occurs as shown in Figure 3f. After the droplet pinches off, the front part of the dispersed liquid thread will continuously flow forward because of its momentum inertia and the drag force from continuous phase, and the remaining part of the liquid thread is retracted backward due to the interfacial tension force. The further breakup of liquid thread occurs, and a satellite droplet is generated as shown in Figure 3g. The interface tension force will retract the liquid thread backward further and the satellite droplet will be transported downstream by the continuous liquid phase as illustrated in Figure 3h.

The front part of the dispersed liquid will expand again as more dispersed liquid flow is continuously injected into the microchannel through the inner capillary nozzle. And the droplet formation process shown in Figure 3 will be repeated to generate droplet periodically. Hence, the droplets produced in each cycle will have similar pattern. For the typical simulation case presented here, as satellite droplets are formed, the final droplets will not be monodisperse. However, the formation of satellite droplets and the primary droplet size can be controlled through adjusting the operation conditions and fluid properties to achieve monodisperse droplets.

Similar simulation results about droplet formation dynamics in a coflowing liquid have been reported in the recent work by Suryo and Basaran.[17] The theoretical analysis of the droplet formation mechanism in a coflowing environment can be also found in the work by Umbanhowar et al.[12] On the basis of the simulation results of the droplet formation process in the dripping mode, the critical point starts with the liquid thread necking as shown in Figure 3d. At this moment, the viscous force from the coflowing liquid just overcomes the interfacial tension force. The viscous force could be estimated using Stokes theory as $F_v \propto C_d\,\mu_o(u_o - u_n)R_n$, and the interface tension force as $F_\sigma \propto \sigma R_n$, where u_n is the flow speed at the neck inside the liquid thread, R_n is the neck radius of liquid thread, and C_d is a coefficient associated with the viscous force. Hence, the ratio of the viscous drag force to the interface tension force is $F_v/F_\sigma = C_d\,\mu_o(u_o - u_n)/\sigma \approx 1$ when the liquid thread necking occurs. Therefore, $u_n \approx u_o - \sigma/C_d\,\mu_o$. Appling the principle of mass conservation to the dispersed liquid phase, the neck radius of the liquid thread can be expressed as $R_n^2 \propto Q_i/\pi u_n \approx Q_i/\pi(u_o - \sigma/C_d\,\mu_o)$. Hence, the droplet radius has the scaling as $R_d \propto R_n \propto (u_o - \sigma/C_d\,\mu_o)^{-1/2}$, when the dispersed liquid phase flow rate (Q_i) is fixed.

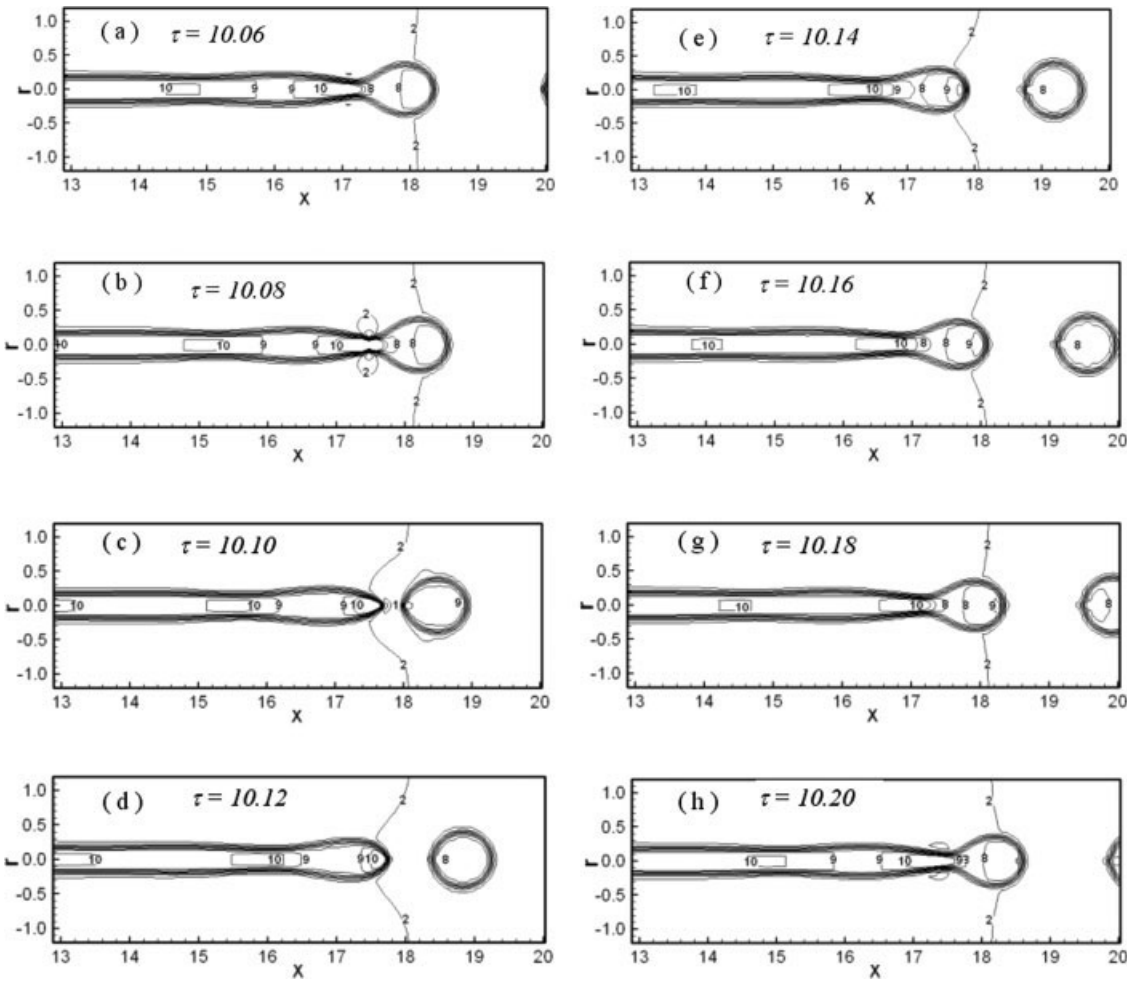

Figure 5. A zoom in view of temporal variation of the pressure field while droplet pinch off in the jetting mode for the coflowing liquids.

The traveling of capillary wave along the jet is captured in the simulation, which matches the end pinch of liquid jet and droplet formation. The flow parameters are as follows: $\overline{u}_i = 1.0$, $\overline{u}_o = 9.5$, $Re^* = 0.1$, $We^* = 0.001$, $\rho^* = 0.8$, $\mu^* = 1.5$ and $R_o/R_i = 3.0$.

Figure 4 shows a typical droplet generation process in coflowing fluids in the jetting mode under the flow conditions $\overline{u}_i{}^* = 1.0, \overline{u}_o{}^* = 10.0, Re^* = 0.1, We^* = 0.001, \rho^* = 0.8$, $\mu^* = 1.5$ and $R_o/R_i = 3.0$. As the continuous phase flow speed increases, the flow momentum of the dispersed fluid phase will be increased as well due to the viscous force, and the disperse liquid phase will finally overcome the capillary pressure inside the liquid thread, leading to a long stretched filament. Finally, the combining effects of viscous force and capillary instability cause the end-pinching of droplet from the liquid filament. A detailed end-pinching process is predicted in the simulation and illustrated in Figure 5 by showing the temporal variation of pressure distribution both inside the liquid filament and in the environmental coflowing liquid. Ten contour levels between the maximum and minimum pressure values are shown in Figure 5. The maximum pressure is found inside the dispersed liquid filament where a thread neck is formed, and the lower pressure exists inside the continuous liquid phase. A high pressure-gradient occurs across the interface. The capillary waves propagate along the liquid filament downstream. When they arrive at the end of the filament, an end liquid bulb is formed and then pinched off as a droplet.

The droplet formation mechanism in the flow-focusing devices has been studied numerically and analyzed theoretically by Zhou et al.[18] The droplet formation in the jetting mode is dominated by the competition between two time scales: a capillary time t_c for the growth of interfacial disturbance and a flow time t_f for the convection of the fluid. If $t_c > t_f$, the capillary disturbance is carried downstream before it is amplified and a droplet gets pinched off. In our case, the capillary time[12,26] can be also estimated as $t_c \propto (\rho_i R_j^3/\sigma)^{1/2}$, where R_j is the jet radius. We take t_f to be the time needed for the wave to travel one wave length downstream, $t_f = \lambda_w/V_w$, where λ_w and V_w are the capillary wave length and wave speed. It can be noted in the simulation that the wave speed is roughly equal to the interfacial speed, which depends strongly upon the continuous phase flow speed u_o. Hence, $t_f \propto \lambda_w/u_o$. The ratio of the capillary time to the flow time can be expressed as

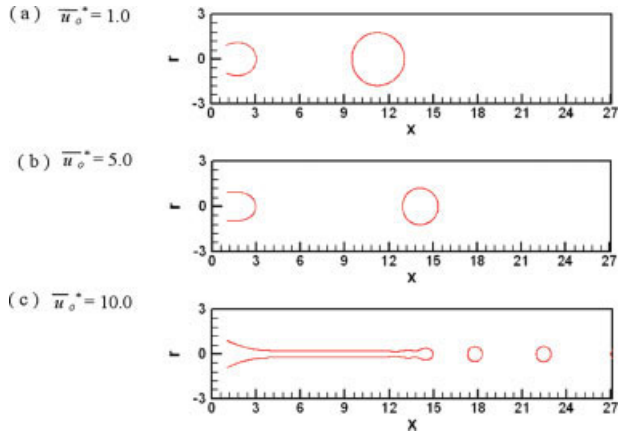

Figure 6. Snapshots showing the droplet formation under different flow speeds of continuous liquid phase.

(a) $\overline{u}_o = 1.0$, (b) $\overline{u}_o = 5.0$, and (c) $\overline{u}_o = 10.0$, while other parameters are kept constant $\overline{u}_i = 1.0$, $Re^* = 0.1$, $We^* = 0.001$, $\rho^* = 0.8$, $\mu^* = 1.5$ and $R_o/R_i = 3.0$. [Color figure can be viewed in the online issue, which is available at www.interscience.wiley.com.]

$(t_c/t_f)^2 \propto \rho_i R_j^3 u_o^2/\sigma\lambda_w^2$. There are a number of reports[31,32] on the gravitational capillary wave studies, but very few reports[33,34] on the capillary wave length caused by viscous drag on a cylindrical immiscible liquid–liquid interface. The size of droplet pinched off from a jet is predicted to be scale with the jet diameter linearly,[18] and hence it can be estimated as $R_d \propto R_j \propto (\sigma\lambda_w^2/\rho_i u_o^2)^{1/3}$.

The above simulation results and analysis demonstrate that the droplet formation dynamics in coflowing fluids depends strongly upon the viscous drag acting on the fluid interface and the capillary instability. Hence, the effects of flow rate and viscosity of the continuous liquid phase, as well as the interface surface tension, on the size of droplets formed in a coflowing liquid are further investigated numerically in the following sections.

Effect of the flow rate of the continuous liquid phase

The simulation results show that the flow speed of the continuous liquid phase has significant effect on the droplet formation. Figure 6 shows the several snapshots of the droplets generated under different average flow speeds of continuous liquid phase in the outer annulus (a) $\overline{u}_o^* = 1.0$, (b) $\overline{u}_o^* = 5.0$, and (c) $\overline{u}_o^* = 10.0$. The average flow speed of the inner dispersed liquid phase is fixed and set to be $\overline{u}_i^* = 1.0$. Other parameters are also fixed, e.g., $Re^* = 0.1$, $We^* = 0.001$, $\rho^* = 0.8$, $\mu^* = 1.5$, and $R_o/R_i = 3.0$. Figure 6 shows that smaller sized droplets are formed when the speed of the continuous liquid phase is increased. This is because the higher speed of the continuous liquid phase induces a higher velocity gradient on the liquid interface and a higher viscous force, which causes the breakup of liquid thread into smaller droplets.

To obtain a correlation of the droplet size with the outer liquid flow rate, a number of simulations are performed by varying the nondimensional flow rate in the range $2 < \overline{u}_o^* < 20$, which leads to the variations of the nondimensional numbers as $0.03 < Ca_o < 0.3$, $0.0032 < We_o < 0.32$, and $0.10 < Re_o < 1.0$. Figure 7 shows the effects of the continuous phase flow rate on the size of droplet formed in the coflowing system. A sharp transition of droplet forming mode is observed when the continuous phase liquid flow speed is about 9.5. During the transition of droplet formation mode there is a sudden drop of the droplet size. The sharp transition of the droplet generation mode from dripping and jetting by adjusting the liquid flow rate has also been observed and reported in the experimental works of Cramer et al.[11] and Utada et al.[6] On the basis of the simulation results, the dependence of droplet size on the continuous phase flow speed can be correlated using curve fitting, and a power law correlation $r_d^* \propto \overline{u}_o^{*-0.48}$is obtained for the dripping mode, and $r_d^* \propto \overline{u}_o^{*-0.73}$ for the jetting mode.

Effect of the viscosity ratio

The viscous force acted on the liquid interface depends strongly upon the viscosities of liquids. The effects of liquid viscosity ratio on droplet formation are studied by varying the viscosity of the continuous phase only and keeping the viscosity of the dispersed phase fixed. The viscosity ratio of the continuous phase to the dispersed phase is varied at (a) $\mu^* = 0.5$, (b) $\mu^* = 2.0$, and (c) $\mu^* = 4.0$. Other parameters are kept constant as: $\overline{u}_i^* = 1.0$, $\overline{u}_o^* = 7.0$, $Re^* = 0.1$, $We^* = 0.001$, $\rho^* = 0.8$, and $R_o/R_i = 3.0$. The simulation predicted snapshots of the droplets generated such flow conditions are shown in Figure 8. When the continuous phase has a higher viscosity, the viscous drag force on the liquid interface should be higher also. This high viscous force will induce a liquid thread from the base cone jet attached to the capillary nozzle (as shown in Figure 8c), and the liquid thread will break into smaller droplets as well as satellite droplets due to capillary instability. On the other hand, when

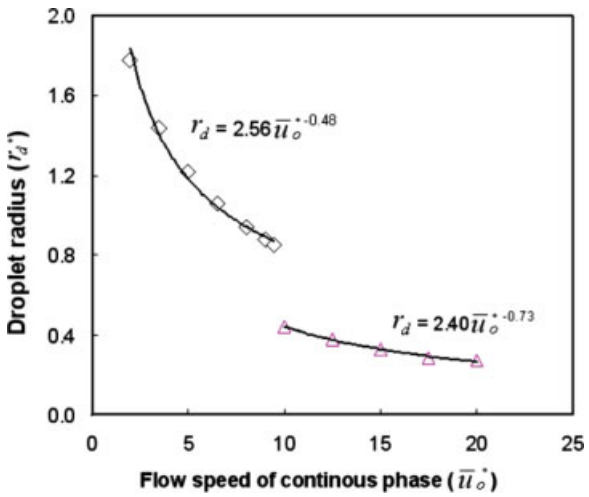

Figure 7. Effect of the flow speed of continuous liquid phase on droplet sized formed in the coflowing system.

The flow speed of the continuous phase is varied from 2 to 20, while other parameters are kept constant $\overline{u}_i = 1.0$, $Re^* = 0.1$, $We^* = 0.001$, $\rho^* = 0.8$, $\mu^* = 1.5$ and $R_o/R_i = 3.0$. [Color figure can be viewed in the online issue, which is available at www.interscience.wiley.com.]

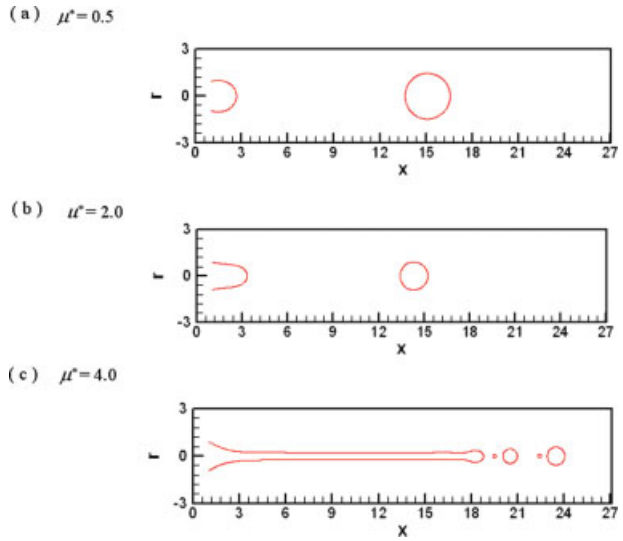

Figure 8. Snapshots showing the droplet formation under different viscosity ratios.

(a) $\mu^* = 0.5$, (b) $\mu^* = 2.0$, and (c) $\mu^* = 4.0$, while other parameters are kept constant $\overline{u}_i = 1.0$, $\overline{u}_o = 7.0$, $Re^* = 0.1$, $We^* = 0.001$, $\rho^* = 0.8$, and $R_o/R_i = 3.0$. [Color figure can be viewed in the online issue, which is available at www.interscience.wiley.com.]

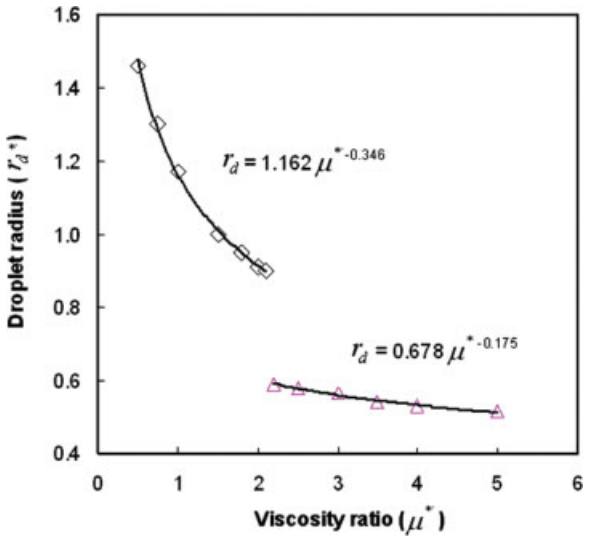

Figure 9. The effect of viscosity ratios on droplet size formed in the coflowing system.

The viscosity ratio is varied from 0.5 to 5, while other parameters are kept constant $\overline{u}_i = 1.0$, $\overline{u}_o = 7.0$, $Re^* = 0.1$, $We^* = 0.001$, $\rho^* = 0.8$, and $R_o/R_i = 3.0$. [Color figure can be viewed in the online issue, which is available at www.interscience.wiley.com.]

the continuous phase has lower viscosity, the interfacial tension will help to stabilize the droplet growth, and larger droplet will be formed.

To correlate the droplet size with the viscosity ratio, a series of simulations are performed by varying the viscosity ratio in the range $0.5 < \mu^* < 5$. The corresponding variation of Reynolds number is in the range of $0.112 < Re_o < 1.12$, Capillary number $0.035 < Ca_o < 0.35$, and Weber number $We_o = 0.0392$. Figure 9 shows the variation of droplet size with the viscosity ratio. It can be noticed from Figure 9 that the droplet formation mode (dripping or jetting mode) can also be observed in the simulations through adjusting the viscosity of the continuous phase liquid. A sharp transition of the droplet generation mode from dripping to jetting is also predicted in the simulation. On the basis of the simulation results, the dependence of droplet size on the viscosity ratio can be correlated using power law fitting as $r_d^* \propto \mu^{*-0.345}$ for the dripping mode and $r_d^* \propto \mu^{*-0.175}$ for the jetting mode.

Effect of the interface tension

The interfacial tension is of great importance in influencing the breakup behavior of disperse liquid droplet in micro channels. In the study, the flow parameter of the inner disperse liquid phase is fixed, and the effects of the interface tension can be investigate by varying the Weber number as defined in Eq. 9. Figure 10 illustrates the snapshots of droplet formation under different interfacial tension as indicated by Weber number (a) $We^* = 0.0005$, (b) $We^* = 0.001$, and (c) $We^* = 0.0015$, while other parameters are kept the same as $\overline{u}_i{}^* = 1.0$, $\overline{u}_o{}^* = 7.0$, $Re^* = 0.1$, $\rho^* = 0.8$, $\mu^* = 1.5$ and $R_o/R_i = 3.0$. When the Weber number is decreased, the corresponding interfacial tension will increase. The stronger interface tension will hold the droplet to the exit of capillary nozzle. As more inner liquid is pumped out, the liquid interface front will grow outward. The area of the interface between the two liquid phases will increased as well, and higher viscous force will be obtained on the liquid droplet. When the droplet size is large enough, the viscous force will overcome the interfacial tension. Finally the droplet will be pinched off from the capillary nozzle and form a droplet with a larger size.

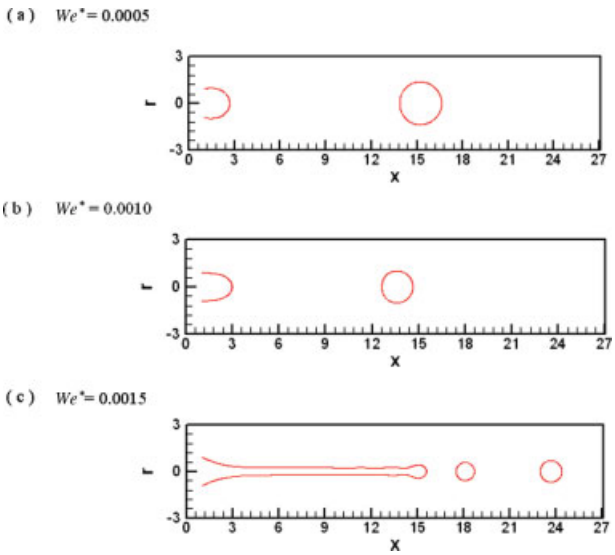

Figure 10. Snapshots showing the droplet formation under different interface surface tension.

(a) $We^* = 0.0005$, (b) $We^* = 0.001$, and (c) $We^* = 0.0015$, while other parameters are kept constant $\overline{u}_i = 1.0$, $\overline{u}_o = 7.0$, $Re^* = 0.1$, $\rho^* = 0.8$, $\mu^* = 1.5$, and $R_o/R_i = 3.0$. [Color figure can be viewed in the online issue, which is available at www.interscience.wiley.com.]

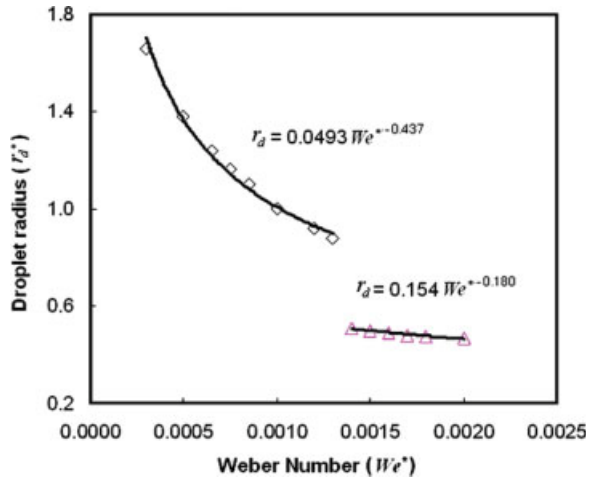

Figure 11. The effect of surface tension on droplet size formed in the coflowing system.

The surface tension (We^*) is varied from 0.0001 to 0.002, while other parameters are kept constant $\overline{u} = 1.0$, $\overline{u}_o = 7.0$, $Re^* = 0.1$, $\rho^* = 0.8$, $\mu^* = 1.5$, and $R_o/R_i = 3.0$. [Color figure can be viewed in the online issue, which is available at www.interscience.wiley.com.]

Effect of the surface tension on the droplet size was studied by varying the Weber number within the range $0.001 < We^* < 0.002$ in the simulation. In this case, the corresponding Capillary number will be in the range of $0.0105 < Ca_o < 0.21$, and Weber number in the range of $0.0039 < We_o < 0.078$, and constant Reynolds number $Re_o = 0.37$. The variation of the droplet size with the Weber number is shown in Figure 11. As shown in Figure 11, it is obvious that the droplet formation mode can also be affected by the surface tension, and that two modes of droplet formation are also predicted. The dependence of droplet size upon the Weber number is correlated using power law fitting as $r_d \propto We^{*-0.437}$ for the dripping mode and $r_d \propto (We)^{*-0.180}$ for the jetting mode based on the simulation results.

Scaling analysis of the continuous phase flow parameters on droplet generation

As presented in the previous sections, it is noted that the dispersed liquid droplet can be formed in a coflowing system. Two droplet forming modes, namely dripping mode and jetting mode, can be caused by controlling the continuous phase flow speed, viscosity, or interface tension. The dependences of the droplet size upon the continuous phase flow parameters such as flow rate, viscosity ratio, and interfacial tension has been analyzed independently in the previous sections. They can be fitted well using power law curve fitting. In fact, for a practical coflowing system, the effects of these parameters may interact with each other. Hence, it is essential to find out the correlations of droplet size with the physical dimensionless parameters such as Reynolds number, Weber number, and Capillary number, where are commonly used to characterize the droplet formation in the microscale channels.

The drop formation dynamics in the faucet dripping into a stationary air environment has been extensively studied by Basaran's group.[14,15,26,27] In their studies, the drop formation is dominated by the capillary, gravitational, and inertial forces. While in the coflowing system, the drop formation is dominated by the capillary, viscous, and inertial forces. A number of the previous studies have been reported about the correlation of droplet size on the flow rate ratio of the two fluid flows in the flow focusing or coflowing system. Experimental studies by Ganan-Calvo[35] on the monodisperse microbubbling generation by capillary flow focusing showed $d_b/D \propto (Q_g/Q_l)^{0.4}$, where d_b, D are the diameters of microbubble and nozzle orifice respectively, and Q_g, Q_l are the flow rates of gas and liquid through the orifice, respectively. This correlation is valid for the case with high Reynolds number (typical from 10^2 to 10^3) and the viscous term is ignored. Zhou et al.[18] studied the droplet formation in the flow focusing devices by numerical simulation. Their analysis showed that the ratio of the diameters of the dispersed liquid filament (r_f) and the nozzle orifice (a) obeys the following power law with the ratio of the inner and outer liquid flow rates: $r_f/a \propto (Q_i/Q_o)^{1/2}$ in the dripping regime. However, the microdroplet size produced in the flow focusing device does not scale with $(Q_i/Q_o)^{1/2}$ due to the flow expansion in the collection tube. In the current study on droplet formation in coflowing immiscible liquids, the droplet formation is mainly dominated by the capillary force and viscous force in the dripping mode, which can be represented by $R_d \propto (u_o - \sigma/C_d\,\mu_o)^{-1/2}$ as discussed in the previous section. If Capillary number ($Ca_o = \frac{(\overline{u}_o \mu_o)}{\sigma}$) is used to characterize the multiphase flow system, we can obtain $R_d \propto (1 - 1/C_d Ca_o)^{-1/2} u_o^{-1/2}$. The power law correlation $r_d^* \propto \overline{u}_o^{*-0.48}$ obtained in the current simulation agrees well with the scaling analysis result $r_d^* \propto \overline{u}_o^{*-1/2}$ for the dripping mode, when we account for the effect of the continuous phase flow speed.

The numerical analysis by Zhang and Stone[7] studied the drop formation at the tip of a vertical, circular capillary tube immersed in a second immiscible liquid for low-Reynolds-number flow using boundary integral method. Their simulation results indicated that the primary drop volume (V_d) decreases as the Bond number increase $V_d \propto Bo^{-0.9}$, where $Bo = \rho g R_o^2/\sigma$, and R_o is the nozzle radius. Theoretical results based on static analysis shows that the critical drop radius is $R_d = (3\sigma/16 R_o^2 \rho g)^{1/3}$, Nondimensionalization gives $R_d \propto Bo^{-1/3}$. Moreover, Garstecki et al.[13,36] studied the microbubble formation in the flow-focusing device, and found that the bubble size is not affected by the interfacial tension substantially. Therefore, the effects of interfacial tension on droplet formation depend strongly upon the flow scenarios. Our analysis of droplet formation in coflowing immiscible liquids presented in the previous section shows $R_d \propto (u_o - \sigma/C_d\,\mu_o)^{-1/2}$. Unfortunately, we do not have a reasonable estimation of the viscous force coefficient (C_d) on the liquid thread. Hence, it is difficult to draw any correlation between droplet diameter and interface tension. From the current simulation results, it is revealed that the droplet size scales as $r_d^* \propto We^{*-0.437}$. It may be approximately expressed as $r_d^* \propto We^{*-1/2}$ based on the above analysis.

Garstecki et al.[13,36] studied the microbubble formation in the flow-focusing device. Jensen et al.[30] performed the numerical simulation of the two-phase stokes flow in an axisymmetric flow-focusing device. They derived the scaling laws for the volume of the created bubble as $V_d \propto 1/\mu_o Q_o$, where μ_o and Q_o is the liquid viscosity and flow rate respec-

tively. Hence, the bubble diameter scales as $D_b \propto \mu_o^{-1/3}$. In the current simulation, the power scaling law of the droplet radius with the viscosity ratio $r_d^* \propto \mu^{*-0.346}$ is reasonable captured for the dripping mode. It can be approximately expressed as $r_d^* \propto \mu^{*-1/3}$, when the inner fluid viscosity is kept constant.

On the basis of the above scaling analysis, the size of the droplet formed in a coflowing liquid system can correlate with the operation parameters approximately as $r_d^* \propto \bar{u}_o^{*-1/2}$, $r_d^* \propto \mu^{*-1/3}$, and $r_d^* \propto We^{*-1/2}$ for the dipping mode. Combining the effects from the three parameters such as the flow speed, viscosity, and interfacial tension, we may obtain the relationship for the dripping mode as $r_d^* \propto \bar{u}_o^{*-1/2}\,\mu^{*-1/3} We^{*-1/2} \approx Ca_o^{-1/2} Re_o^{-1/6}$. Figure 12a shows the variation of nondimensional droplet size with the combined dimensionless parameter $(Ca_o^{-1/2} Re_o^{-1/6})$ for all the simulation cases with the dripping mode presented in the previous sections. It is interesting to notice that the droplet size correlates with the combined dimensionless parameter $(Ca_o^{-1/2} Re_o^{-1/6})$ linearly for all the simulation cases under the dripping mode. It also indicates that the droplet formation in the dripping mode could be dominated by the balance between the capillary force and viscous force.

The scaling analysis in the previous section shows that $R_d \propto (\sigma \lambda_w^2/\rho_i u_o^2)^{1/3}$ for the jetting mode. The dependency of droplet size and continuous phase speed is as $R_d \propto u_o^{-2/3}$ if the capillary wave length is a function of surface tension and viscosity and remained constant. In the review work by Lasheras and Hopfinger[37] on the liquid jet instability and atomisation in a coaxial gas stream, the liquid core length (L) can be estimated using capillary wave theory as $L/D_l = C(\rho_l u_l^2/\rho_g u_g^2)^{2/3}(\sigma/\mu_l u_l)^{1/3}$, where D_l is the nozzle diameter of liquid jet, and C is an adjustable constant, and subscript l and g represent the liquid and gas phases, respectively. The shorter liquid core length means that the shear viscous force is stronger to break up the jet, and the droplets produced will be finer. In our immiscible coflowing liquid system, the abovementioned formation can be used to estimate the jet breaking length (L_b) as $\frac{L_b}{R_j} = C(1/\rho_o u_o^2)^{2/3}(\sigma/\mu_o)^{1/3}$ when the inner liquid has a fixed flow rate. The droplet volume may scale with the jet break length as $R_d^3 \propto R_j L_b$. As $R_d \propto R_j$, the droplet size may scale as $R_d \propto L_b^{1/2} \propto u_o^{-2/3}\sigma^{1/6}\mu_o^{-1/6}$. The simulation results show that $r_d^* \propto \bar{u}_o^{*-0.73}$, $r_d^* \propto \mu^{*-0.175}$, and $r_d^* \propto We^{*-0.180}$. Combining the effects from the three parameters of flow speed, viscosity, and interface tension, we may obtain the relationship, $r_d^* \propto \bar{u}_o^{*-0.73}\,\mu^{-0.175} We^{*-0.180}$. And this correlation can be estimated approximately as $r_d^* \propto \bar{u}_o^{*-2/3}$ $\mu^{*-1/6} We^{*-1/6}$, and re-expressed in the physical dimensionless numbers as $r_d^* \propto Ca_o^{1/3}\, We_o^{-1/2}\mu^{*-1/2}$. Figure 12b shows the variation of droplet size with the combined dimensionless parameter $(Ca_o^{1/3} We_o^{-1/2}\,\mu^{*-1/2})$ for all the simulation cases with the jetting mode presented in the previous sections. Although the droplet size correlates with the combined dimensionless number linearly with almost same slope for the all simulation cases, they deviate from each other with certain shifting. The challenges in correlating the droplet size with the operation parameters for the coflowing system in the jetting mode come from the difficulties to estimate the capillary wave length along the immiscible liquid–liquid interface. In addition, because of the large aspect ratio of the jet (small in diameter and large in jet length), it is also a challenge in simulation to achieve high resolution in both time and space domains to capture the details about the capillary wave and droplet pinch-off dynamics.

Conclusion

The drop formation of a disperse liquid injected into another coflowing immiscible liquid within a microchannel is simulated numerically using front tracking method to investigate the drop formation mechanism. The understanding of such droplet formation mechanism is very critical to the design of microfluidic devices to generate monosized droplets in a controllable manner. The key phenomena in the droplet formation process, such as liquid drop growth, neck-

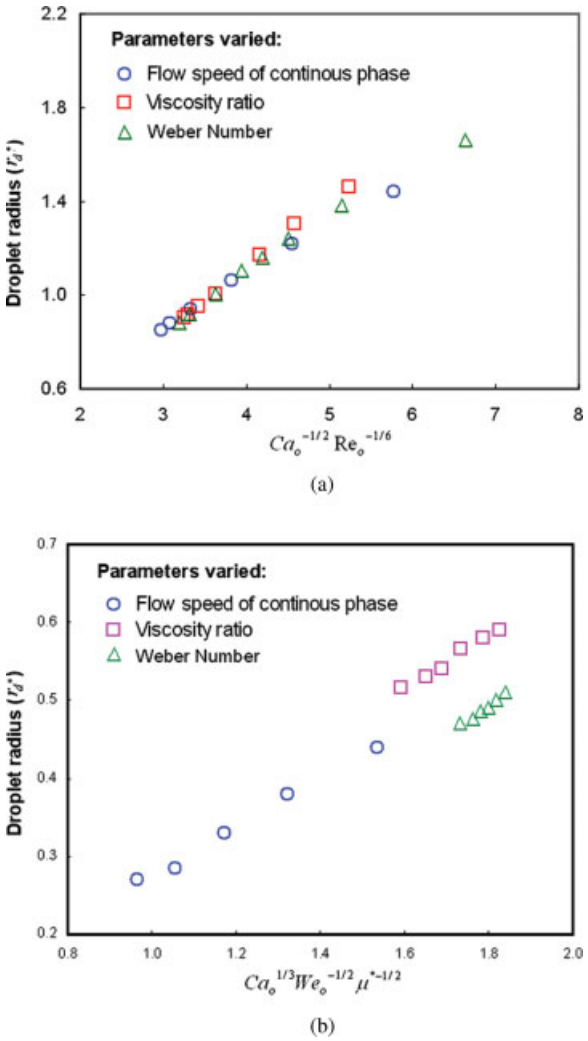

Figure 12. Scaling analysis on the size of droplet formed in the coflowing system at (a) dripping mode and (b) jetting mode under the effects of different continuous phase flow speed, fluid viscosity, and interface tension.

[Color figure can be viewed in the online issue, which is available at www.interscience.wiley.com.]

ing, breakup of primary drop, and satellite drop formation, are reasonably captured. In addition, the effects of some important parameters of flow conditions and fluid property, such as continuous liquid phase flow speed, viscosity, and interface tension, on the size of droplet formed in the microchannel were also studied. It is found that there are two kinds of droplet forming modes, namely dripping and jetting mode, depending upon the flow conditions. The droplet size correlated with the continuous phase flow parameters as $r_d \propto Ca_o^{-1/2}\ Re_o^{-1/6}$ under dripping mode and as $r_d \propto Ca_o^{1/3}\ We_o^{-1/2}\mu^{*-1/2}$ under jetting mode.

The simulation results indicates that the droplet formation in coflowing system depend strongly on the balance between the viscous shear force from the continuous phase flow and interface tension force on the droplet. The higher flow speed and viscosity normally generates higher shear viscous drag force on the droplet, which helps drop breakup from the capillary exit and form smaller droplets. On the other hand, the higher interface tension (i.e., lower Weber number) may delay the droplet breakup from the capillary exit. And hence, more disperse liquid is accumulated in the droplet, and the final detached droplet normally has large size. From this study, it can also be concluded that the coflowing system in microchannel has good mechanism to control the size of the droplet produced, and could produce same size droplet periodically.

Acknowledgments

The authors express special thanks to Dr. Evert Klaseboer and Dr. Shaoping Quan for the constructive discussions and valuable suggestions.

Notation

Ca = capillary number, dimensionless
Bo = bond number, dimensionless
$D(\ )$ = distribution function, dimensionless
g = gravitational acceleration, m^2/s
h = grid size of background mesh, m
$I(\ )$ = fluid indicator function, dimensionless
$\mathbf{n}$ = unit outer pointed normal vector on interface, dimensionless
p = static pressure, Pa
Q = volume flow rate of fluid, m^3/s
r = radial distance, m
r_d^* = droplet radius, dimensionless
R = radius of tube, m
Re = reynolds number, dimensionless
$\mathbf{t}$ = unit tangential vector on interface, dimensionless
t = time, s
$\mathbf{u}$ = fluid velocity, m/s
U = axial component of fluid velocity, m/s
V = radial component of fluid velocity, m/s
u = axial component of fluid velocity, dimensionless
v = radial component of fluid velocity, dimensionless
$\mathbf{X}$ = position of the interface, dimensionless

Greek letters

Δd = interface breakup distance in simulation
$\delta()$ = dirac delta function
κ = curvature of interface, m^{-1}
λ_w = capillary wave length, m
μ = fluid viscosity, Pa·s
ρ = fluid density, kg/m^3
σ = interface tension, N/m
τ = dimensionless time

Subscript/superscript symbol

f = interface
i = inner tube/liquid phase
n = time step in the simulation or the neck of liquid thread
o = outer tube/liquid phase
$*$ = nondimensionalised parameter
$\bar{}$ = area averaged parameters

Literature Cited

1. Basaran OA. Small-scale free surface flows with breakup: drop formation and Emerging Applications. *AIChE J*. 2002;48:1842–1846.
2. Barrero A, Loscertales IG. Micro- and nanoparticles via capillary flows. *Annu Rev Fluid Mech*. 2007;39:89–106.
3. Anna SL, Bontoux N, Stone HA. Formation of dispersions using 'flow focusing' in micro-channels. *Appl Phys Lett*. 2003;82:364–366.
4. Xu Q, Nakajima M. The generation of highly monodisperse droplet through the breakup of hydrodynamically focused microthread in a microfluidic device. *Appl Phys Lett*. 2004;85:3726–3728.
5. Xu S, Nie Z, Seo M, Lewis P, Kumacheva E, Stone HA, Garstecki P, Weibel DS, Gitlin I, Whitesides GM. Generation of monodisperse particles by using micro-fluidics: control over size, shape, and composition. *Angew Chem Int Ed*. 2005;44:724–728.
6. Utada AS, Lorenceau E, Link DR, Kaplan PD, Stone HA, Weitz DA. Monodisperse double emulsions generated from a micro capillary devices. *Science*. 2005;308:537–541.
7. Zhang D, Stone HA. Drop formation in viscous flows at a vertical capillary tube. *Phys Fluids*. 1997;9:2234–2242.
8. Zhang X, Basaran OA. An experimental study of dynamics of drop formation. *Phys Fluids*. 1995;7:1184–1203.
9. Zhang X. Dynamics of drop formation in viscous flows. *Chem Eng Sci*. 1999;54:1759–1774.
10. Zhang X. Dynamics of growth and breakup of viscous pendant drops into air. *J Colloid Interface Sci*. 1999;212:107–122.
11. Cramer C, Fischer P. Windhab EJ. Drop formation in a coflowing ambient fluid. *Chem Eng Sci*. 2004;59:3045–3058.
12. Umbanhowar PB, Prasad V, Weitz DA. Monodisperse emulsion generation via drop break off in a coflowing stream. *Langmuir*. 2000;16:347–351.
13. Garstecki P, Stone HA, Whitesides GM. Mechanism for flow-rate controlled break-up in confined geometries: a route to monodisperse emulsions. *Phys Rev Lett*. 2005;94:164501.
14. Wilkes ED, Phillips SD, Basaran OA. Computational and experimental analysis of dynamics of drop formation. *Phys Fluids*. 1999; 11:3577–3598.
15. Chen AU, Notz PK, Basaran OA. Computational and experimental analysis of pinch-off and scaling. *Phys Rev Lett*. 2002;88:174501.
16. Davidson MR, Harvie DJE, Cooper-White JJ. Flow focusing in microchannels. *ANZIAM J*. 2005;46(E):C47–C58.
17. Suryo R, Basaran OA. Tip streaming from a liquid drop forming from a tube in a coflowing outer fluid. *Phys Fluids*. 2006;18:082102.
18. Zhou C, Yue P, Feng JJ. Formation of simple and compound drops in microfluidic devices. *Phys Fluids*. 2006;18:092105.
19. Unverdi SO, Tryggvason G. A front-tracking method for viscous, incompressible, multi-fluid flows. *J Comput Phys*. 1992;100:25–37.
20. Hua J, Lou J, Murali K, Lee KH, Kumar K. Simulation of bubble rise and deformation in liquid using a front tracking/finite difference method. Proceedings of third International Symposium on Computational Technologies for Fluid/Thermal/Chemical Systems with Industrial Applications, Atlanta, USA, 22–26 July 2001,225–234.
21. Hua J, Lou J. Numerical simulation of bubble rising in viscous liquid. *J Comput Phys*. 2007;222:769–795.
22. Patankar SV. *Numerical Heat Transfer and Fluid Flow*. New York: Hemisphere, 1980.
23. Clift R, Grace JR, Weber ME. *Bubbles, Drops, and Particles*. New York: Academic Press, 1978.
24. Peskin CS, Printz BF. Improved volume conservation in the computation of flows with immersed boundaries. *J Comput Phys*. 1993;105:33–46.
25. Bunner B, Tryggvason G. Dynamics of homogenous bubbly flows, Part 1: rise velocity and microstructure of the bubbles. *J Fluid Mech*. 2002;466:17–52.

26. Ambravaneswaran B, Subramani HJ, Phillips SD, Basaren OA. Dripping-jetting transitions in a dripping faucet. *Phys Rev Lett*. 2004;93: 034501.
27. Subramani HJ, Yeoh HK, Suryo R, Xu Q, Ambravaneswaran B, Basaran OA. Simplicity and complexity in a dripping faucet. *Phys Fluids*. 2006;18:032106.
28. Burton JC, Waldrep R, Taborek P. Scaling and instability in bubble pinch-off. *Phys Rev Lett*. 2005;94:184502.
29. Homma S, Koga J, Matsumoto S, Song M, Tryggvason G. Breakup mode of an axisymmetric liquid jet injected into another immiscible liquid. *Chem Eng Sci*. 2006;61:3986–3996.
30. Jensen MJ, Stone HA, Bruus H. A numerical study of two-phase Stokes flow in an axisymmetric flow-focusing device. *Phys Fluids*. 2006;18:077103.
31. Sferrazza M, Xiao C, Jones RAL. Evidence for capillary waves at immiscible polymer/polymer interfaces. *Phys Rev Lett*. 1997;78:3693–3696.
32. Gondret P, Rabaud M. Shear instability of two-fluid parallel flow in a Hele-Shaw cell. *Phys Fluids*. 1997;9:3267–3274.
33. Liberzon D, Shemer L, Barnea D. Upward-propagating capillary waves on the surface of short Taylor bubbles. *Phys Fluids*. 2006;18: 048103.
34. Powers T, Zhang D, Goldstein RE, Stone HA. Propagation of a topological transition: the Rayleigh instability. *Phys Fluids*. 1998;10: 1052–1057.
35. Ganan-Calvo AM. Perfectly monodisperse microbubbling by capillary flow focusing: an alternate physical description and universal scaling. *Phys Rev E*. 2004;69:027301.
36. Garstecki P, Gitlin I, DiLuzio W, Whitesides GM. Formation of monodisperse bubbles in a microfluidic flow-focusing device. *Appl Phys Lett*. 2004;85:2649–2651.
37. Lashera JC, Hopfinger EJ. Liquid jet instability and atomization in a coaxial gas stream. *Ann Rev Fluid Mech*. 2000;32:275–308.

Manuscript received Dec. 17, 2006, and revision received July 20, 2007.